

Exclusive J/ψ and Υ production in high energy pp and $p\text{Pb}$ collisions

C. A. Flett^{a,b}, S. P. Jones^c, A. D. Martin^c, M. G. Ryskin and T. Teubner^d

^a*Department of Physics, University of Jyväskylä, P.O. Box 35, 40014 University of Jyväskylä, Finland*

^b*Helsinki Institute of Physics, P.O. Box 64, 00014 University of Helsinki, Finland*

^c*Institute for Particle Physics Phenomenology, Durham University, Durham, DH1 3LE, U.K.*

^d*Department of Mathematical Sciences, University of Liverpool, Liverpool, L69 3BX, U.K.*

Abstract

We present a formalism for determining the cross section for exclusive heavy vector meson production (J/ψ , Υ) as a function of rapidity, in both high energy proton-proton and proton-heavy ion collisions, at next-to-leading order in QCD. We compare and contrast the production in pp and $p\text{Pb}$ collisions and show how data for these processes can give information on the low x gluon distribution of the proton and heavy ions at a range of different scales.

1 Introduction

There is a long history of experimental and theoretical study of exclusive vector meson production in high-energy proton-proton collisions. In particular, data for the differential cross section $d\sigma(p + p \rightarrow p + V + p)/dY$ has come under theoretical scrutiny for vector mesons $V = J/\psi, \Upsilon(1S)$, where the $+$ signs denote large rapidity gaps between the rapidity Y of the vector meson and the outgoing protons, ensuring the exclusivity of the experimental measurements. The theoretical description proceeds by first calculating the differential cross section for the exclusive photoproduction subprocess $\gamma + p \rightarrow V + p$ for which the dominant QCD diagram is sketched in simplified form in Fig. 1. At high energy the process is driven by the behaviour of the gluon parton distribution of the proton at small momentum fraction. In this work, we

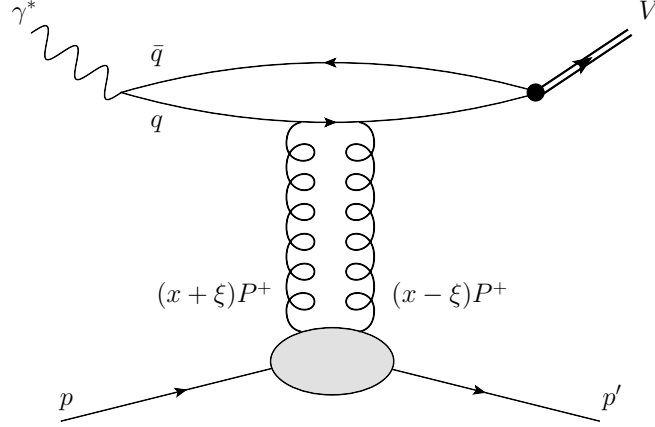


Figure 1: A schematic diagram of high-energy exclusive vector meson production, $\gamma^* + p \rightarrow V + p$. The factorized form follows since, in the proton rest frame, the formation time $\tau_f \simeq 2E_\gamma/(Q^2 + M_V^2)$ is much greater than the $q\bar{q}$ -proton interaction time. Q is the virtuality of the photon and the lightcone momentum $P^+ = (p + p')/2$. For the photoproduction set-up considered here, we have $Q^2 = 0$.

apply the theoretical framework, based on collinear factorisation and developed to NLO in perturbative QCD in [1, 2], to p Pb collisions. Other approaches include, for example, models based on the Colour-Glass-Condensate (CGC) [3, 4] and k_T -factorisation frameworks [5], as well as LO perturbative QCD [6]. Note that the two exchanged gluons in Fig. 1 carry different fractions of the incoming proton momentum, so we are dealing with a generalised, skewed gluon distribution. The net momentum fraction transferred from the proton to the vector meson is 2ξ , thus for this exclusive process 2ξ plays the role of the usual variable ‘ x ’ in DIS. For our high energy process we have $x - \xi \ll x + \xi \ll 1$ and the cross section can be accurately estimated in terms of the conventional gluon distribution $g(2\xi)$ and a skewing correction [7, 8]. Recall that a detailed NLO analysis of the current inclusive data determines the NLO gluon distribution down to $2\xi \simeq 10^{-4}$ [9]. For smaller momentum fractions the uncertainties become too large, see also [10]. However, the exclusive J/ψ data from LHC [11, 12] are found to determine the gluon distribution down to $2\xi \sim 3 \times 10^{-6}$.

In Section 2 we note that in going from the cross section for photoproduction, $\gamma + p \rightarrow V + p$, to that for $p + p \rightarrow p + V + p$, we need to allow for photon emissions from both incoming protons. Moreover, we have to evaluate the photon flux and the survival factors of the rapidity gaps, i.e. the probabilities that the rapidity gaps do not get populated by additional emissions. Section 3 concerns exclusive vector meson production in p Pb collisions. Data for such a process appear to have the advantage of having a much larger cross section; enhanced by the large charge of the heavy Pb ion, that is by a factor $Z^2 = 6724$. However, when we come to evaluate the cross section we find the theoretical formalism is much more complicated than that for pp collisions. In Section 4 we compare the differential cross section data from ALICE and CMS

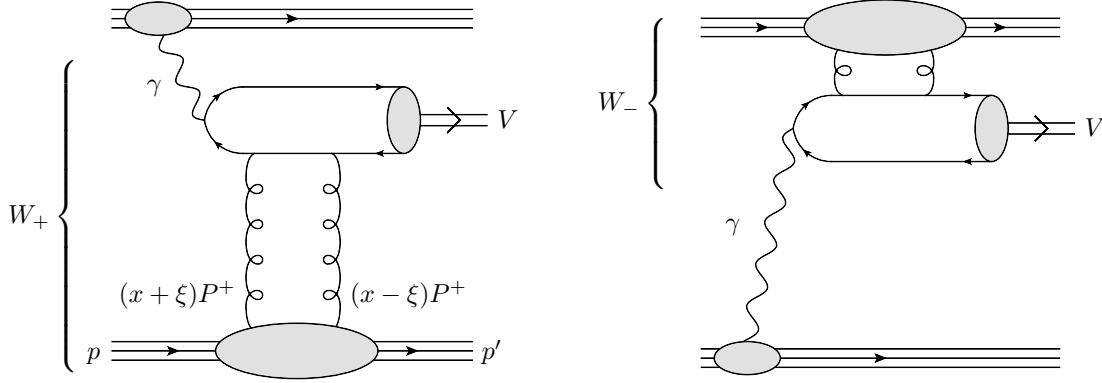


Figure 2: The two diagrams describing exclusive heavy vector meson production in $p+p \rightarrow p+V+p$, at the LHC. The W_+ and W_- contributions arise in the ultraperipheral description of the $\gamma + p \rightarrow V + p$ subprocess, see the text for details. In the $p\text{Pb}$ mode, either the upper or lower proton is replaced by a Pb-ion.

at the proton-nucleon collision energy $\sqrt{s_{pN}} = 5.02$ TeV for the process $p + \text{Pb} \rightarrow p + V + \text{Pb}$, where $V = J/\psi, \Upsilon$, with our corresponding theoretical results. We then provide predictions at $\sqrt{s_{pN}} = 8.16$ TeV, before presenting our conclusions and outlook in Section 5.

2 Exclusive $p + p \rightarrow p + V + p$ production

We begin with pp collisions, and leave the discussion of $p\text{Pb}$ collisions until the next section. The procedure for calculating the cross section for the high-energy exclusive process $p+p \rightarrow p+V+p$ (where the vector meson $V = J/\psi$ or Υ and where the $+$ signs represent rapidity gaps) is described in [5, 13]. As mentioned above, we first calculate the cross section for the exclusive photoproduction process

$$\sigma_W(\gamma p) \equiv \sigma(\gamma + p \rightarrow V + p) \quad (1)$$

where W is the γp centre-of-mass energy. This process is driven by the two amplitudes sketched in Fig. 2. In the left diagram the photon is radiated by the upper proton and then the vector meson, V , is created on the lower proton via the $\gamma + p \rightarrow V + p$ reaction. The diagram on the right shows the other possibility where the photon is emitted from the lower proton while the upper proton acts as the target.

When the meson V is detected in the forward region, the corresponding γp energies are quite different

$$W_+^2 = M_V \sqrt{s} e^Y \quad \text{and} \quad W_-^2 = M_V \sqrt{s} e^{-Y}, \quad (2)$$

where Y is the rapidity of the vector meson in the laboratory (i.e. pp centre-of-momentum) frame. Since the $\gamma p \rightarrow V + p$ cross section steeply grows with energy, the dominant contribution comes from the first amplitude which corresponds to a larger energy W_+ .

The cross section for exclusive V production in ultraperipheral pp collisions is therefore given by the sum¹ of the exclusive photoproduction cross sections, $\sigma_{\pm}(\gamma p)$ of eqn. (1), at the two γp energies W_{\pm}

$$\frac{d\sigma(p + p \rightarrow p + V + p)}{dY} = S^2(W_+) \left(k_+ \frac{dn_p}{dk_+} \right) \sigma_+(\gamma p) + S^2(W_-) \left(k_- \frac{dn_p}{dk_-} \right) \sigma_-(\gamma p). \quad (3)$$

Note that the subprocess cross sections are weighted by the survival factors $S^2(W_{\pm})$ which account for the probability that the rapidity gap between the vector meson and the target proton is not populated by soft interactions which would destroy the exclusivity of the event; and by the photon fluxes dn_p/dk_{\pm} for photons of energy $k_{\pm} = x_{\pm}\sqrt{s}/2$, where x_{\pm} are the fractions of the parent proton energy carried by the photon.

The flux of photons emitted from a proton is well known [14]

$$\frac{dn_p(x)}{dx} = \frac{\alpha^{\text{QED}}}{\pi^2 x} \int \frac{d^2 q_{\perp}}{q_{\perp}^2 + x^2 m_p^2} \left(\frac{q_{\perp}^2}{q_{\perp}^2 + x^2 m_p^2} (1-x) F_E(Q^2) + \frac{x^2}{2} F_M(Q^2) \right), \quad (4)$$

where q_{\perp} is the photon transverse momentum, m_p is the proton mass and $F_{E,M}$ are the proton form factors

$$F_E(Q^2) = (4m_p^2 G_E^2(Q^2) + Q^2 G_M^2(Q^2)) / (4m_p^2 + Q^2), \quad (5)$$

$$F_M(Q^2) = G_M^2(Q^2). \quad (6)$$

The scale $Q^2 = (q_{\perp}^2 + x^2 m_p^2) / (1-x)$, while G_E and G_M are the ‘Sachs’ form factors, which may be expressed in dipole forms

$$G_E(Q^2) = 1 / (1 + Q^2 / 0.71 \text{GeV}^2)^2, \quad (7)$$

$$G_M(Q^2) = 2.79 / (1 + Q^2 / 0.71 \text{GeV}^2)^2. \quad (8)$$

The rapidity gap survival factors, $S^2(W_{\pm})$, are calculated in impact parameter, b , space using

$$S^2(W_{\pm}, b) = \exp(-\Omega(b, W_{\pm})), \quad (9)$$

where $\Omega(b, W)$ is the opacity (i.e. optical density) of the proton-proton interaction at the energy W and the vector valued impact parameter $\mathbf{b} = (b_x, b_y)$, see e.g. [15].

The results as a function of the rapidity of the vector meson are tabulated for different collider energies in [5] and [13] for $V = J/\psi$ and Υ , respectively.

¹The interference between the two amplitudes of the two subprocesses is small since the transverse momentum of the proton which radiates the photon is much smaller than that of the target proton. Thus we may neglect the interference term at the accuracy we are aiming at here.

3 Exclusive $p + \text{Pb} \rightarrow p + V + \text{Pb}$ production

In a proton-lead collision the photon flux radiated coherently by the lead ion is strongly enhanced by the factor $Z^2 = 6724$. So, as mentioned before, at first sight the amplitude with the photon emitted by the lead ion (say, Fig. 2 left) should dominate. However the situation is not so simple.

3.1 The different contributions

Firstly, in the $\gamma + \text{Pb} \rightarrow V + \text{Pb}$ process, the nucleons situated at the same impact parameter (i.e. on the line directed along the beam) may interact coherently as well. That is we have a competition between the factor $Z^2 = 6724$ and a coherent factor of about $A^{4/3} = 1232$, see [16] for more details. Thus the proton induced rate is suppressed only by a factor of 5 relative to that induced by Pb.

Moreover, as it is seen from the right hand side of (4), we have essentially a logarithmic integral $\int dq_{\perp}^2/q_{\perp}^2$ in the interval from $q_{\perp} \simeq xm_p$ up to the value $\sim 1/R$ limited by the form factors. That is, within the leading-logarithmic approximation, the photon flux is proportional to $\ln(1/(xm_p R))$, where $x_{\pm} = (M_V/\sqrt{s})e^{\pm Y}$ is the proton momentum fraction carried by the photon and R is the radius of the photon emitter. Thus, for a large rapidity Y , the flux radiated by the proton may be enhanced by the ratio

$$\ln(1/(x_- m_p R_p)) / \ln(1/(x_+ m_p R_{\text{Pb}})), \quad (10)$$

which for an Υ at $Y = 2.5$ reaches 6.8 at $\sqrt{s} = 14$ TeV. Here $(xm_p)^2$ is the minimal virtuality squared, $|t_{\min}|$, of the photon which carries the fraction x of the momentum of the parent proton. The crucial point is that to produce a heavy Υ at large Y the photon must carry a large fraction of the nucleon beam momentum and the value of xm_p becomes comparable to the inverse ion radius, $1/R_{\text{Pb}}$. That is the logarithm in the denominator of the ratio becomes small.

Besides this, the amplitude where the photon was radiated by the proton may be enhanced due to the energy dependence of the elementary photoproduction amplitude.

Therefore, it is not evident that it is sufficient to consider only the photons radiated by the heavy ion. In particular, for the case of forward exclusive Υ production in the lead ion direction, the contribution caused by the photon radiated off the proton beam may even dominate at large Y . In our computations we will keep both amplitudes. The kinematic configurations are illustrated (see Fig. 9) and discussed in Appendix B.

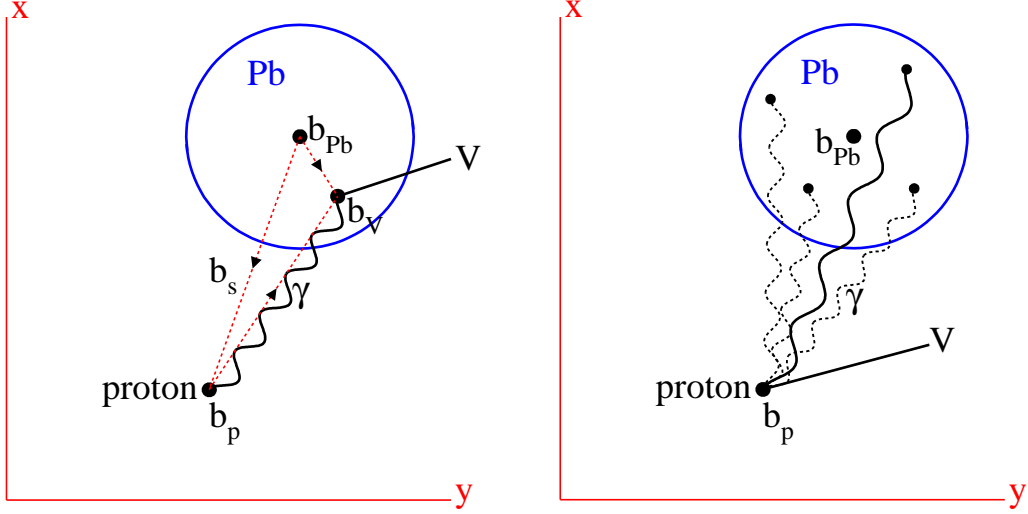


Figure 3: The geometry of the $p + \text{Pb} \rightarrow p + V + \text{Pb}$ process in the transverse (x, y) plane. In the left diagram the photon is radiated off the incoming proton, whereas in the right diagram the photons are radiated by the lead ion. The black dotted curves indicate that we add coherently the contributions of each proton inside the lead ion. Note that the photons can be emitted and absorbed at different points along the z beam axis.

3.2 Including the probability of rapidity gap survival

Here we recall the structure of the calculations needed to account for the gap survival probability in *exclusive* vector meson production in $p\text{Pb}$ collisions. We will follow Section 6 of [16], see also [17].

It is convenient to work in terms of the transverse coordinate; that is, to work in the two-dimensional impact parameter b space. Let us start with the incoherent production of the vector meson in proton-ion collisions in which the photon is emitted from the incoming proton. The situation is sketched in Fig. 3(a). The figure shows the impact factors \mathbf{b}_{Pb} , \mathbf{b}_p and \mathbf{b}_V corresponding respectively to the centre of the Pb ion, the proton and the produced vector meson. Note that we show the extent in b space of the Pb ion. It is convenient to take the vertex of the meson production to be the origin of the transverse plane, that is to take $\mathbf{b}_V = \mathbf{0}$.

Since we are looking for the cross section ($\sigma \propto \mathcal{A}^* \mathcal{A}$) integrated over the momentum transferred t , the values of b are the same in the \mathcal{A}^* and \mathcal{A} amplitudes. Allowing for the photon flux and survival factors, we can therefore write the expression for the cross section of the *incoherent* $p + \text{Pb} \rightarrow p + V + \text{Pb}$ interaction (for the case of the photon radiated by the incoming proton) as

$$\sigma_{\text{incoh}} = \int d^2 b_p d^2 b_{\text{Pb}} T(b_{\text{Pb}}) \frac{x dn_p(x, b_p)}{dx} |\mathcal{A}|^2 S_p^2(b_s) S_V^2(b_{sv}), \quad (11)$$

where $n_p(x, b)$ is the flux of photons emitted off the proton, $\mathcal{A} = \mathcal{A}(W, b_a)$ is the $\gamma + p \rightarrow V + p$ amplitude in b representation and $T(b_{\text{Pb}})$ is the optical density of the Pb ion, evaluated as given

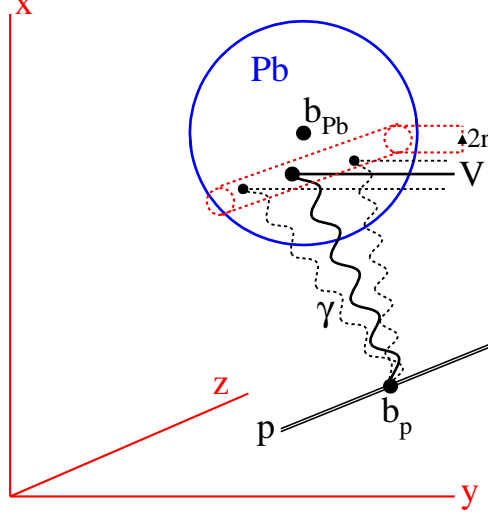


Figure 4: The geometry of the $p + \text{Pb} \rightarrow p + V + \text{Pb}$ process, where (x, y) is the transverse plane and z is in the direction of the beam. The black dotted curves indicate that we add coherently the contributions of each nucleon absorbing a photon inside the lead ion tube of the radius $r = \sqrt{4B_V}$ directed along the beam (z) axis. The transverse size of tube, r , is driven by the t -slope (i.e. the size) of the $\gamma + N \rightarrow V + N$ amplitude. The extra factor $4\pi B_V T(b_{\text{Pb}})$ in (15) in comparison with (11) is the number of nucleons which may act coherently inside this tube of transverse area $4\pi B_V$. Note that the photons can be emitted and absorbed at different points along the z beam axis.

in the Appendix A. Equation (11) is written in the limit of a small size amplitude \mathcal{A} , i.e. the size of the amplitude given by the t -slope $B_V = B_0 + 4\alpha' \ln(W/W_0)$, see later, is much less than that for the heavy ion $R_{\text{Pb}}^2 \gg 4B_V$.² The survival factors are

$$S_p^2(b_s) = \exp(-T(b_s)\sigma(pN)) , \quad (12)$$

which is the probability not to fill the gap by secondary emissions produced in additional proton-lead interactions, where $b_s = |\mathbf{b}_{\text{Pb}} - \mathbf{b}_p|$, and

$$S_V^2(b_{sv}) = \exp(-T(b_{sv})\sigma(VN)) , \quad (13)$$

which is the probability not to fill the gap by secondaries produced in additional vector meson-Pb interactions, where $b_{sv} = |\mathbf{b}_{\text{Pb}} - \mathbf{b}_V| = b_{\text{Pb}}$ with our choice $\mathbf{b}_V = \mathbf{0}$. Finally, $\sigma(pN)$ (and $\sigma(VN)$) are the cross sections of the proton-nucleon (vector meson-nucleon) interaction inside the ion. Recall that the expressions (12, 13) are similar to the probability not to have an additional interaction in the target and the product $T(b)\sigma$ plays the role of the optical density of the target, that is the opacity Ω in (9).

²Accounting, however, for the non-locality of \mathcal{A} in the computation, i.e. the size of the proton, we replace the optical density $T(b)$ (30) by the convolution $T(b) = \frac{1}{4\pi B_V} \int d^2b' T(b') \exp[-(\mathbf{b} - \mathbf{b}')^2/(4B_V)]$. Analogous replacements (with the corresponding B slopes) were used in the calculation of the survival factors S^2 . For proton-nucleon interactions the slope $B_{\text{el}} = 20 \text{ GeV}^{-2}$ is used for $\sqrt{s_{pN}} = 8.16 \text{ TeV}$ and $B_{\text{el}} = 19.1 \text{ GeV}^{-2}$ for $\sqrt{s_{pN}} = 5.02 \text{ TeV}$.

If we were to neglect the survival factors (i.e. setting $S^2 = 1$) then the cross section would be

$$\sigma_{\text{incoh}} = \frac{xdn_p(x)}{dx} \sigma(\gamma + p \rightarrow V + p) \cdot A, \quad (14)$$

where $A = 208$ is the lead atomic number.

As mentioned above, besides the incoherent interaction, we need to consider coherent production as well. Here the situation is sketched in Fig. 4. The *coherent* cross section is of the form

$$\sigma_{\text{coh}} = 4\pi B_V F_{\text{Pb}}^2(t_{\text{min}}) \int d^2b_p d^2b_{\text{Pb}} T^2(b_{\text{Pb}}) \frac{xdn_p(x, b_p)}{dx} |\mathcal{A}|^2 S_p^2(b_s) S_V^2(b_{\text{Pb}}), \quad (15)$$

where the dimension of the extra T factor is compensated by the t -slope of the $\gamma + p \rightarrow V + p$ amplitude³. The amplitude \mathcal{A} is normalized to $\int d^2b |\mathcal{A}(b)|^2 = \sigma(\gamma + p \rightarrow V + p)$.

The form factor F_{Pb} in (15) accounts for the nucleon distribution in the lead ion. The point is that the coherence of the interaction with different nucleons should not be destroyed by the longitudinal component of the momentum transferred. This component is represented by $t_{\text{min}} = -(xm_p)^2/(1-x)$. Since the value of $|t_{\text{min}}|$ is small in our kinematics, here we use just the exponential parametrization $F_{\text{Pb}}(t) = \exp(\langle r_{\text{Pb}}^2 \rangle t/6)$, with $\langle r_{\text{Pb}}^2 \rangle$ being the mean radius squared of the lead ion.

We are particularly interested in the case when the photons are radiated by the lead ion. Then we have only coherent radiation to consider. Here the situation is sketched in the right panel of Fig. 3. Now the cross section has the form

$$\sigma_{\text{Pb}} = \sigma(\gamma + p \rightarrow V + p) \int d^2b_{\text{Pb}} \frac{xdn_{\text{Pb}}(x, b_{\text{Pb}})}{dx} S_p^2(b_{\text{Pb}}) S_V^2(b_{\text{Pb}}). \quad (16)$$

Calculating the photon flux, $n(x, b)$, given by (4) we keep just the electric (F_E) term since the magnetic (F_M) contribution contains an additional x^2 factor, while we work at small x . Besides this, the magnetic contribution is concentrated at low impact parameters where the gap survival factor S_p^2 is extremely small. (We have checked that the magnetic (F_M) contribution does not exceed 1%.) For the lead ion the form factor F_E corresponds to the proton distribution in lead, see (31).

Note, however, that expression (4) cannot be transformed to the coordinate, b , representation directly. First, we have to transform the *amplitude* of photon emission and to account for the polarization structure of the amplitude. The point is that the photon polarization vector \mathbf{e}_γ is directed parallel to the photon transverse momentum \mathbf{q}_\perp . That is, the amplitude should be a vector. In b space it will be the vector $\mathbf{a}_\gamma = \mathbf{b} a(b)$. Calculating the Fourier transform gives

$$\mathbf{b} a(b) = \frac{1}{4\pi^2} \int \frac{d^2q_\perp e^{i\mathbf{b} \cdot \mathbf{q}_\perp}}{(q_\perp^2 + x^2 m_p^2)} \mathbf{q}_\perp \sqrt{\frac{\alpha^{\text{QED}}}{\pi x}} (1-x) F_E(Q^2), \quad (17)$$

³Recall that the t behaviour of the photoproduction cross section $d\sigma(\gamma + p \rightarrow V + p)/dt \propto \exp(B_V t)$ corresponds to the amplitude $\mathcal{A}(b) = \mathcal{A}(b=0) \exp[-b^2/(2B_V)]$.

and after the angular integration we do not obtain the usual zero-order Bessel $J_0(\mathbf{b} \cdot \mathbf{q}_\perp)$, but rather $J_1(\mathbf{b} \cdot \mathbf{q}_\perp)$ [18]. Since $J_1(\mathbf{b} \cdot \mathbf{q}_\perp)$ vanishes as $b \rightarrow 0$, the typical values of the impact parameter become larger.

Finally the photon flux in the b representation outside the heavy ion takes the form

$$\frac{d^3 n_{\text{Pb}}}{dx d^2 b_\gamma} = \frac{Z^2 \alpha^{\text{QED}}}{x \pi^2 b_\gamma^2} (x m_p b_\gamma)^2 K_1^2(x m_p b_\gamma), \quad (18)$$

where $K_1(z)$ is the modified Bessel function.

3.3 The uncertainty in the evaluation of S^2

Note that the expression for S_V in (13) is written in the spirit of the vector meson dominance (VMD) model [19, 20]. That is, we *assume* that the photon to Υ transition takes place *before* the collision and then the *completely dressed* Υ meson interacts with the heavy ion. This is reasonable when the meson goes in the proton beam direction (see [21] for a detailed discussion). However, the assumption is not justified for a very forward (large rapidity) Υ going in the direction of the lead ion. Indeed, the $\gamma \rightarrow b\bar{b}$ vertex is point-like and for $Y > 2 - 3$ the quarks do not have sufficient time to form the normal Υ wave function. From the beginning the size of the $b\bar{b}$ pair is too small, and the corresponding cross section [22, 23]

$$\sigma(VN) \propto \alpha_s^2 \langle r_{b\bar{b}}^2 \rangle \quad (19)$$

is smaller than the cross section of the normally dressed Υ meson.

In addition, the absorption cross section for the Υ meson, $\sigma(VN)$, is not known experimentally. Moreover it depends on the VN collision energy $s_{VN} = W^2$. For our numerical estimate we take the Regge behaviour

$$\sigma_{VN}(W) = \sigma_0 \left(\frac{W^2}{M_V^2} \right)^{\alpha_P(0)-1} \quad (20)$$

and assume that $\sigma_0 \propto 1/M_V^2$. The normalization is fixed to the J/ψ absorptive cross section, $\sigma(J/\psi N) \simeq 4$ mb, at $W \simeq 10$ GeV for a completely dressed J/ψ meson measured by the N50 collaboration [24]. For the Pomeron intercept we take $\alpha_P(0) - 1 = 0.25$. This is consistent with the DIS data and the intercept of the BFKL Pomeron after the resummation of the next-to-leading logarithmic corrections [25, 26, 27, 28]. Since the expected value of $\sigma(\Upsilon N)$ is small, the survival probability due to Υ absorption, S_V^2 , is rather close to unity.

To demonstrate the effect, we compare the obtained results with those taking $\sigma(\Upsilon N) = 0$. The difference never exceeds 6-10%. Accounting for the ‘undressed meson’ problem this means that for the mesons going with large rapidity in the lead ion direction the true value of S^2 may be about 3-5% larger.

Finally, there is some uncertainty due to the value of the proton-nucleon cross section $\sigma(pN)$. Recall that at 8 TeV TOTEM had measured $\sigma_{\text{tot}}(pp) = (103 \pm 2.3)$ mb [29], while ATLAS-ALFA gives (96 ± 1) mb [30]. Here we take $\sigma(pN) = 100$ mb for our numerics. The corresponding uncertainty is about 3-4%.

3.4 Numerical results for (photon flux) \times (gap survival)

For proton-lead collisions, eqn. (3) is replaced by the form

$$\begin{aligned} \frac{d\sigma(p + \text{Pb} \rightarrow p + V + \text{Pb})}{dY} &= S^2(W_{\text{Pb}}) \left(k_+ \frac{dn_{\text{Pb}}}{dk_+} \right) \sigma_{\gamma p}(W_{\text{Pb}}) \\ &+ S^2(W_p) \left(k_- \frac{dn_p}{dk_-} \right) \left(\sigma_{\text{incoh}}(W_p) + \sigma_{\text{coh}}(W_p) \right) R_A^2, \end{aligned} \quad (21)$$

where the nuclear modification factor $R_A(2\xi) = g_{\text{Pb}}(2\xi)/(Ag_p(2\xi))$ accounts for the fact that the gluon distribution⁴ in the lead ion may differ from the sum of the gluon distributions in free nucleons. The value of the nucleon modification factor $R_A(2\xi)$ at the corresponding scale $\mu = M_V/2$ is taken from the EPPS16 NLO analysis [31]. It is convenient to introduce the so-called ‘effective fluxes’, f_{Pb} and f_p , which include the original photon flux $x dn/dx$ times the survival and nuclear modification effects⁵. The effective flux radiated by the lead ion is

$$f_{\text{Pb}}(2\xi) = \frac{\sigma_{\text{Pb}}}{\sigma(\gamma + p \rightarrow V + p)}, \quad (22)$$

where σ_{Pb} is given by (16). The effect of the flux radiated by the proton is given by the sum of coherent and incoherent fluxes,

$$f_{\text{incoh}}(2\xi) = \frac{\sigma_{\text{incoh}}}{\sigma(\gamma + p \rightarrow V + p)} R_A^2(2\xi) \quad (23)$$

and

$$f_{\text{coh}}(2\xi) = \frac{\sigma_{\text{coh}}}{\sigma(\gamma + p \rightarrow V + p)} R_A^2(2\xi), \quad (24)$$

where σ_{incoh} and σ_{coh} are given by (11) and (15), respectively. Here, $2\xi = 2M_V^2/(2W^2 - M_V^2) \approx M_V^2/W^2$ for $W^2 \gg M_V^2$, i.e. $2\xi \ll 1$, is the fractional momentum transfer provided by the two-gluon exchange.

Finally, the cross section of heavy vector meson production can be written as

$$\frac{d\sigma(p + \text{Pb} \rightarrow p + V + \text{Pb})}{dY} = f_{\text{Pb}}(W_{\text{Pb}}) \sigma_{\gamma p}(W_{\text{Pb}}) + \left(f_{\text{incoh}}(W_p) + f_{\text{coh}}(W_p) \right) \sigma_{\gamma p}(W_p). \quad (25)$$

Here the values of W_{Pb} and W_p correspond to the energies of the $\gamma + p \rightarrow V + p$ process initiated by the photon emitted off the lead ion and proton beam, respectively.

The values of the effective fluxes are presented in Tables 1 and 2 in Appendix B for Υ and J/ψ production at proton-nucleon collision energy $\sqrt{s_{pN}} = 5.02$ TeV. The analogous values at $\sqrt{s_{pN}} = 8.16$ TeV are given in Tables 3 and 4.

⁴Recall that the value of $\sigma(\gamma + p \rightarrow V + p) \propto (2\xi g(2\xi))^2$ is almost completely driven by the gluon distribution.

⁵It is not completely correct to use the word ‘flux’ for a quantity which includes these additional effects; however we use it since it enables us to shorten the description of the computations.

4 Comparison with data

In this section, we compare our theoretical predictions with the rapidity differential cross section data from ALICE [32, 33] and CMS [34] for the process $p+\text{Pb} \rightarrow p+V+\text{Pb}$, where $V = J/\psi, \Upsilon$. Using eqn. (25) we compute $d\sigma(p+\text{Pb} \rightarrow p+J/\psi+\text{Pb})/dY$, with $\sigma_{\gamma p}$ evaluated using, as input, the gluon PDF fit obtained from our previous analyses [35].

We work at NLO within the collinear factorisation scheme and express the amplitude for exclusive heavy vector meson photoproduction as

$$\mathcal{A} = \frac{4\pi\sqrt{4\pi\alpha}e_q(\epsilon_V^* \cdot \epsilon_\gamma)}{N_c} \left(\frac{8\langle O_1 \rangle_V}{M_V^3} \right)^{1/2} \int_{-1}^1 dx \left(C_g(x, \xi) F_g(x, \xi) + C_q(x, \xi) F_q(x, \xi) \right), \quad (26)$$

where F_g and F_q are the gluon and quark singlet Generalised Parton Distributions (GPDs), C_g and C_q are the gluon and quark coefficient functions, see [1, 2], and $x - \xi$, $x + \xi$ are the parton momentum fractions in the lightcone direction P^+ . The corresponding gluon and quark coefficient functions for exclusive heavy vector meson electroproduction were calculated in [36, 37]. The dependence on the factorisation and renormalisation scales, μ_F, μ_R , and on the four-momentum transfer squared, t , is not shown. The set-up is illustrated in Fig. 5. The non-relativistic QCD (NRQCD) matrix element $\langle O_1 \rangle_V$ is fixed by the experimental value of the heavy vector meson decay width to a dilepton pair, see [38].

We take $\mu_R = \mu_F$ and use the ‘optimal’ factorization scale $\mu_F = M_V/2$, see [39]. That is, the exclusive J/ψ and Υ photoproduction data probe the gluon densities at two different scales. Besides this, we implement the Q_0 subtraction [2] needed to avoid the double counting between the low $k_T < Q_0$ contributions in the NLO coefficient functions and that hidden in the PDF inputs. This choice provides a sufficiently good scale stability of the prediction⁶.

The cross section, $\sigma_{\gamma p}$, integrated over the Mandelstam variable t , is given by

$$\sigma_{\gamma p}(W) = \frac{1}{B_V(W)} \left(\frac{d\sigma}{dt} (\gamma p \rightarrow V p) \Big|_{t=0} \right) = \frac{1}{B_V(W)} \frac{(\text{Im}\mathcal{A})^2(1+\rho^2)}{16\pi W^4}, \quad (27)$$

where

$$\rho = \frac{\text{Re}\mathcal{A}}{\text{Im}\mathcal{A}} = \tan \left(\frac{\pi}{2} \frac{\partial \ln(\text{Im}\mathcal{A}/W^2)}{\partial \ln W^2} \right) \quad (28)$$

is the real part correction, see e.g. [40], and $B_V(W)$ is the Regge-motivated energy dependent slope parameter given by

$$B_V(W) = \left(B_0 + 4\alpha'_P \ln \left(\frac{W}{W_0} \right) \right) \text{ GeV}^{-2}. \quad (29)$$

Here, $B_0 = 4.9$ for $V = J/\psi$ [41] and $B_0 = 4.63$ for $V = \Upsilon$, with $\alpha'_P = 0.06$ and $W_0 = 90 \text{ GeV}$ [42]. The smaller value of B_0 for the case $V = \Upsilon$ is due to the need for reducing the J/ψ slope parameter by the factor $4\alpha' \ln(M_\Upsilon/M_{J/\psi})$.

⁶Recall that exactly the same approach (that is use of the optimal scale $\mu_F = M_V/2$ and the Q_0 subtraction) was applied in [35] to determine the low- x gluon PDF from exclusive J/ψ data, used in the present analysis.

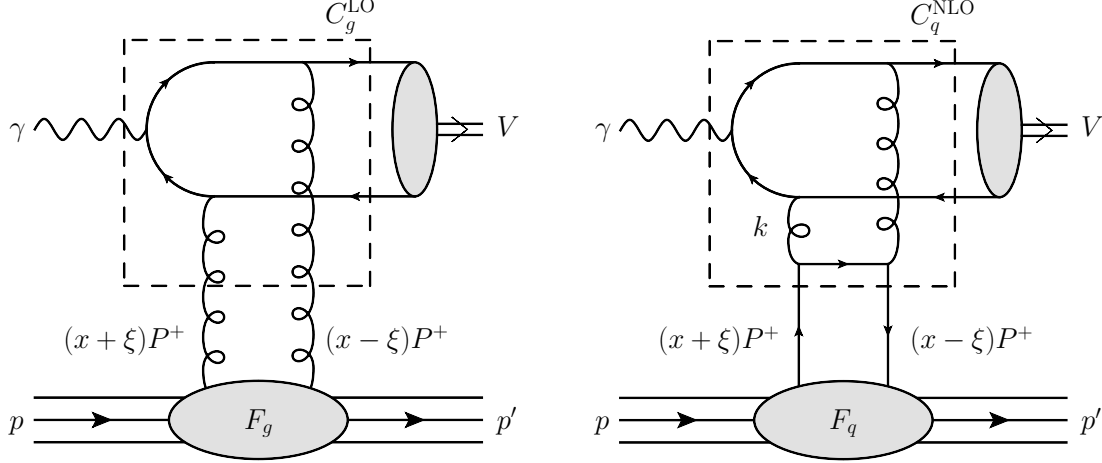


Figure 5: The LO and the NLO quark contributions to $\gamma + p \rightarrow V + p$ amplitude. The parton momentum fractions are $x + \xi$ and $x - \xi$ and k is the loop momentum.

Fig. 6 shows our rapidity differential cross section predictions at $\sqrt{s_{pN}} = 5.02$ TeV for the process $p + \text{Pb} \rightarrow p + V + \text{Pb}$. The upper row shows the predictions for $V = J/\psi$ and the lower one for $V = \Upsilon$. In the left panels, we show the decomposition of the total cross section result into the γp contribution (the first term on the right hand side of eqn. (25), labelled by σ_{Pb} in the figure) and the γPb contribution (the second term on the right hand side of eqn. (25), labelled by σ_p in the figure). In the right panels, we show our results compared with existing data from ALICE and/or CMS [32, 33, 34]. The error bands are indicative of the uncertainty due to our previous low x gluon PDF fit [35] only and does not account for theoretical uncertainties in the present formalism. We emphasise that no fit is performed to the $p\text{Pb}$ data here, and the width of the bands is given by propagating the errors on the fit parameters using the full covariance matrix obtained from our previous gluon PDF fit made to the low x exclusive J/ψ data in pp collisions in [35].

For $V = J/\psi$, the γPb contribution is less than a percent at mid-rapidity, while for $V = \Upsilon$, it is as much as 7%. The mass of the Υ is ~ 3 times that of the J/ψ and so (with $k_+ \propto M_V$ and $W_+ \propto \sqrt{M_V}$), the typical photon energy in exclusive Υ production is now much larger than in exclusive J/ψ production for a given Y_{lab} . Therefore, the photon flux radiated off Pb is relatively suppressed for Υ production. We remark that for $Y_{\text{lab}} < -3$ in Fig. 6c, the photon radiated by Pb has a somewhat greater x (with respect to the nucleon in Pb) and so the value of $b_{\text{Pb}} = b_\gamma$ (in eq. (18)) is rather small. This means that the integrated flux from Pb is not large and $S^2(b_{\text{Pb}})$ is small. On the other hand, the photon radiated by the proton has a much smaller x (with respect to the proton) leading to a larger S^2 and a larger integrated flux. This is evident from Tab. 3 where, for $Y_{\text{lab}} < -3$, the value of f_{Pb} is an order of magnitude smaller than f_p . The energy dependence of $\sigma(\gamma + N \rightarrow V + N)$ does not compensate this difference for $\sqrt{s_{pN}} = 5.02$ TeV. This accounts for the W_p contribution being greater than the W_{Pb} one in this region.

Our predictions agree favourably with the ALICE data, particularly at backward, central

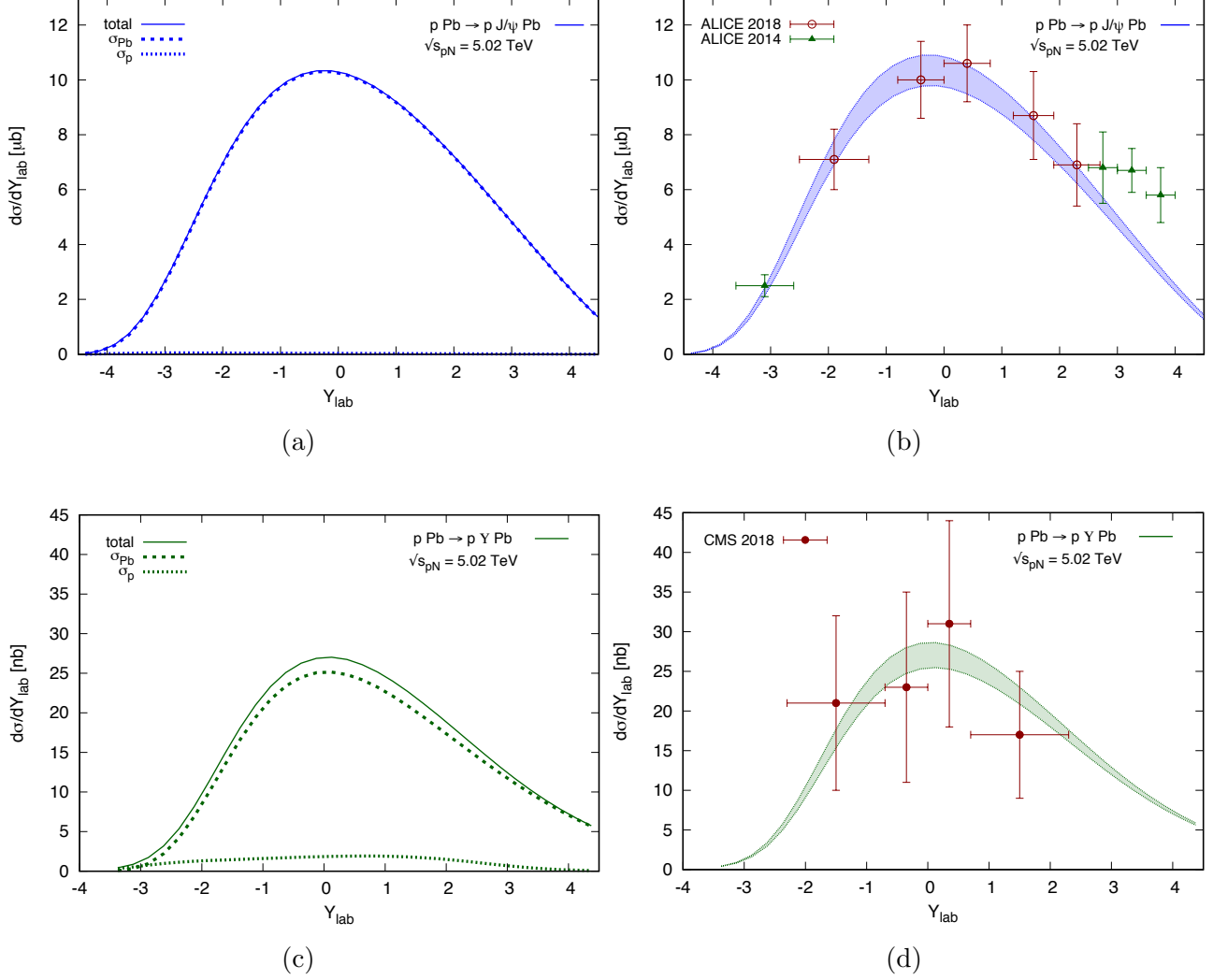


Figure 6: Theoretical predictions for coherent exclusive J/ψ and Υ photoproduction rapidity differential cross sections in $p\text{Pb}$ collisions with $\sqrt{s_{pN}} = 5.02$ TeV. Panels (a) and (c) show the decomposition of the total cross section into the σ_{Pb} and σ_p contributions, see text for details. Panels (b) and (d) compare our predictions with existing data from ALICE and/or CMS [32, 33, 34]. We emphasise that no fit is made to the data shown, the width of the uncertainty bands is obtained by the $\pm 1\sigma$ statistical uncertainties and the normalisation errors of the datasets used in our previous fit [35] to determine the low x gluon PDF, which is used in the present analysis.

and semi-forward rapidities. For $V = J/\psi$, our prediction undershoots the data for $Y_{\text{lab}} \geq 2.5$. In this region, however, our prediction is well constrained. As shown above, the dominant contribution comes from the photon radiated by Pb, occurring at large b , with S^2 very close to unity where we have practically no uncertainty in the photon flux. On the other hand, the ‘gamma-proton’ centre of mass energy is relatively small, and this is precisely the region where our gluon PDF fit agreed well with the HERA data [35]. The earlier ALICE data from [32] for $Y_{\text{lab}} \geq 2.5$ show an unexpected plateauing behaviour and are arguably inconsistent with those in [33]⁷.

In Fig. 7, we show the analogous set of plots at $\sqrt{s_{pN}} = 8.16$ TeV. There are currently no data for $p + \text{Pb} \rightarrow p + V + \text{Pb}$ at this centre-of-mass energy, but forthcoming measurements for the case $V = \Upsilon$ from CMS are anticipated [43, 44]. Our results for the rapidity distribution are qualitatively consistent with the shapes predicted by other approaches, however, the normalisation of our prediction is larger than that obtained from CGC models [3, 4].

In both Figs. 6 and 7, note that the larger $d\sigma/dY_{\text{lab}}$ at positive Y_{lab} is indicative of the proton direction corresponding to the positive Y_{lab} . At negative Y_{lab} the distribution is skewed due to a smaller energy per nucleon in the Pb-ion. Indeed, at large rapidities in the Pb direction (i.e. large negative Y_{lab}), the contribution due to the photon radiated from Pb is strongly suppressed, especially in the Υ case, since the momentum fraction, $x \propto (M_V/\sqrt{s}) \exp(Y)$ carried by the photon becomes large and the transverse momentum cutoff xm_p becomes comparable with the inverse lead ion radius $1/R_{\text{Pb}}$, i.e. here we deal with the impact parameter $b_{\text{Pb}} \sim R_{\text{Pb}}$. Therefore, in this region, the survival factor $S^2(b_{\text{Pb}})$ suppresses the σ_{Pb} contribution, and the second term of (25), i.e. the photons radiated by the proton, starts to dominate.

5 Conclusions

We have predicted the cross sections for exclusive J/ψ and Υ meson production in proton-lead ion collisions at the LHC for centre-of-mass energies $\sqrt{s_{pN}} = 5.02$ TeV and $\sqrt{s_{pN}} = 8.16$ TeV, using the low x gluon distribution extracted in [35] from the data on $p + p \rightarrow p + J/\psi + p$. We account for the gap survival probability caused by both the additional proton-lead interactions and the interaction of the secondary vector meson inside the heavy ion.

As expected, the dominant contribution to the cross section in exclusive $p\text{Pb}$ collisions comes from the amplitude where the photon is radiated by the lead ion (for all rapidities $Y_{\text{lab}} \gtrsim -3$). However, our detailed study finds that the naively expected dominance of the Z^2 enhancement of the cross section, when we go from exclusive production from photons radiated by a proton to that for photons radiated by the heavy ion, is considerably reduced. Nevertheless, we find that the enhancement is still sufficient to enable forthcoming data for exclusive heavy vector meson production in $p\text{Pb}$ collisions to provide additional constraints on the *free* proton gluon

⁷The behaviour of the earlier ALICE data in Fig. 6b are incompatible with other theoretical predictions, too, see e.g. Fig. 4 of [6].

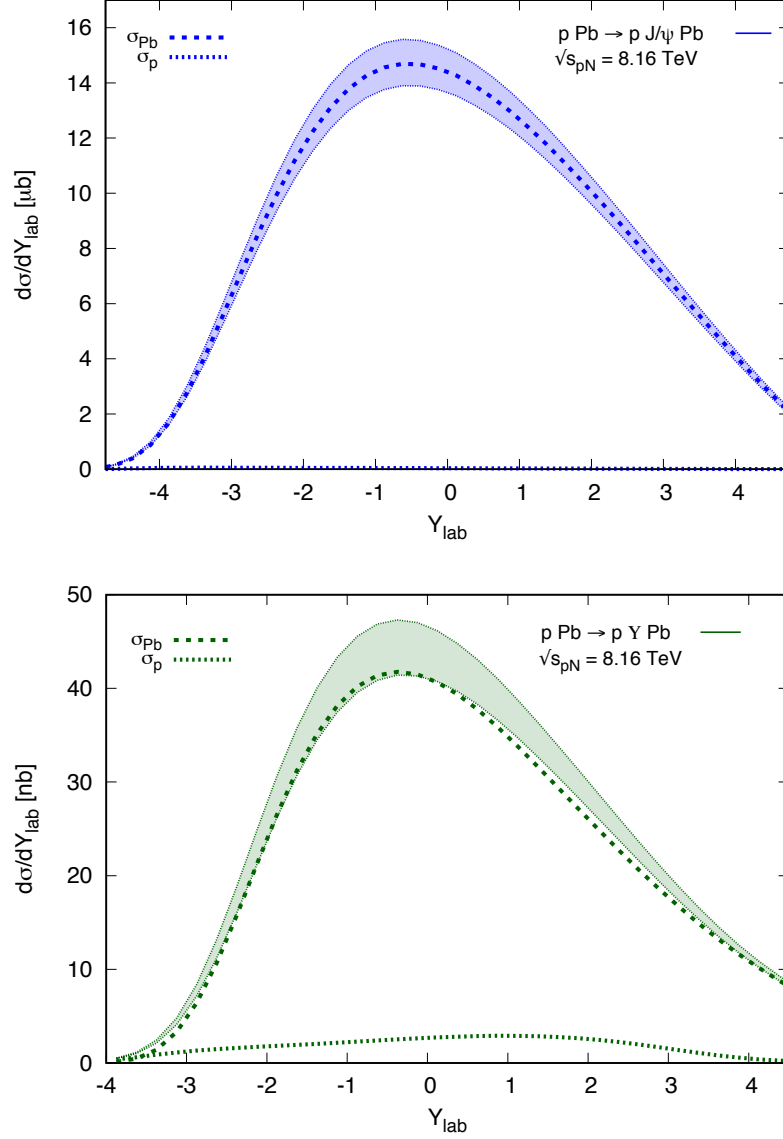


Figure 7: Theoretical predictions for coherent exclusive J/ψ and Υ photoproduction rapidity differential cross sections in $p\text{Pb}$ collisions with $\sqrt{s_{pN}} = 8.16 \text{ TeV}$. The bands and curves are as described in the caption of Fig. 6. Note that currently there are no data for the process $p + \text{Pb} \rightarrow p + V + \text{Pb}$, with $V = J/\psi, \Upsilon$, at this centre-of-mass energy, but measurements for Υ photoproduction are shortly anticipated [43, 44].

PDF at low to moderate values of x and scale. Such data could be used in a combined fit with those in pp collisions anticipated from the High-Luminosity phase of the LHC, as well as in the upcoming ep programme of the Electron-Ion collider, to provide refined constraints on the gluon PDF.

Appendix A: Optical density of the Pb ion

The optical density of the Pb ion may be written in the form

$$T(b_{\text{Pb}}) = \int_{-\infty}^{+\infty} dr_z (\rho_p(r) + \rho_n(r)), \quad (30)$$

with $r = \sqrt{r_z^2 + r_t^2}$. For the nucleon density in lead, $\rho(r)$, we use the Woods-Saxon form [45]

$$\rho_N(r) = \frac{\rho_0}{1 + \exp((r - R)/d)}, \quad (31)$$

where the parameters d and R , respectively, characterise the skin thickness and the radius of the nucleon density in the heavy ion; $r = (r_z, r_t)$. For ^{208}Pb we take the recent results of [46, 47]

$$\begin{aligned} R_p &= 6.680 \text{ fm}, & d_p &= 0.447 \text{ fm}, \\ R_n &= (6.67 \pm 0.03) \text{ fm}, & d_n &= (0.55 \pm 0.01) \text{ fm}. \end{aligned} \quad (32)$$

The nucleon densities, ρ , are normalized to

$$\int \rho_p(r) d^3r = Z, \quad \int \rho_n(r) d^3r = N_n, \quad (33)$$

for which the corresponding proton (neutron) densities are $\rho_0 = 0.063$ (0.093) fm^{-3} .

Appendix B: Tables of effective fluxes

The values of the effective fluxes used in eqn. (25) are presented in Tables 1 and 2 below for Υ and J/ψ production at proton-nucleon collision energy $\sqrt{s_{pN}} = 5.02$ TeV. The analogous values at $\sqrt{s_{pN}} = 8.16$ TeV are also given, in Tables 3 and 4.

The first column is the rapidity, Y_{lab} , of the vector meson measured in the laboratory frame. We account for the asymmetry of proton-ion collisions. In the case of lead we have (in the laboratory frame) a proton beam momentum equal to 4 TeV (6.5 TeV), while the momentum of a nucleon in lead is 4 (Z/A) = 1.58 TeV (6.5 (Z/A) = 2.56 TeV) for $\sqrt{s_{pN}} = 5.02$ (8.16) TeV. Positive $Y_{\text{lab}} > 0$ corresponds to the vector meson going in the proton direction.

The second and fourth columns are the γ -nucleon collision energies W_{Pb} and W_p . The effective flux f_{Pb} is given in the third column while the fluxes f_{incoh} , f_{coh} and their sum are shown in the fifth, sixth and seventh column, respectively.

Column eight gives the sum $f_{\text{incoh}} + f_{\text{coh}}$ for the case $R_A = 1$. The factor of R_A enters only the term where the photon is radiated by the proton and, as shown in Figs. 6 and 7, this contribution is relatively small (especially for J/ψ) and can be seen at large backward rapidities only. The contribution due to the term where the photon is radiated from the proton with and without inclusion of the nuclear modification factor, R_A , is shown in Fig. 8. This difference at the total cross section level amounts to at most a few percent only for the J/ψ case because the

contribution when the photon is radiated from the lead ion dominates. Therefore, the nuclear modification factor is hardly seen in $p\text{Pb}$ collisions, where the first term of (25) dominates. This factor can be much better observed (and measured) in the Pb-Pb set-up, see e.g. [48] for a baseline description of the $\text{Pb} + \text{Pb} \rightarrow \text{Pb} + J/\psi + \text{Pb}$ process in the collinear factorisation framework to NLO.

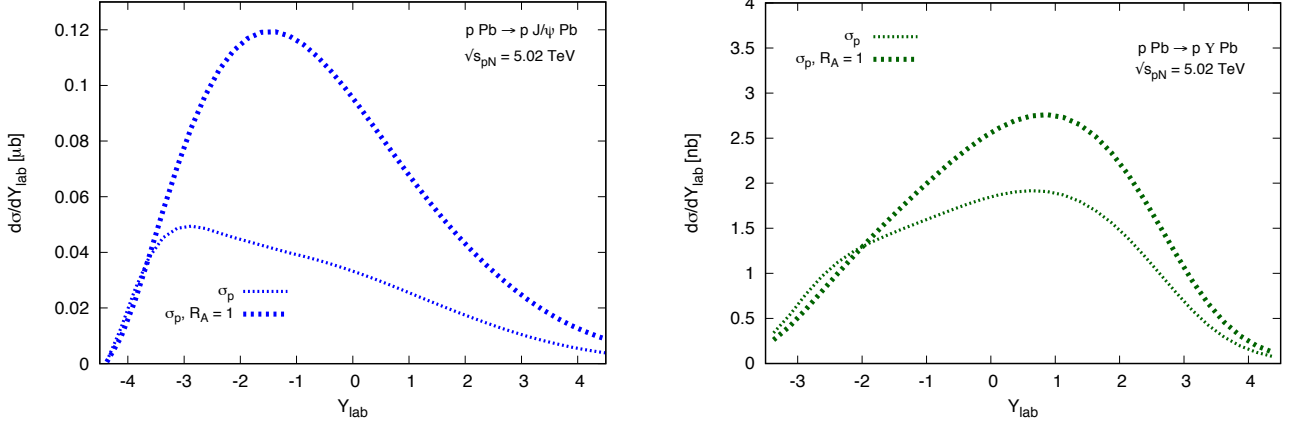


Figure 8: The contribution due to the term where the photon is emitted from the proton, σ_p , with and without inclusion of the nuclear modification factor, R_A . The left panel is for the J/ψ production at $\sqrt{s_{pN}} = 5.02$ TeV and the right panel is for Υ production at the same centre-of-mass energy.

Note that in asymmetric $p\text{Pb}$ collisions, the laboratory frame does not coincide with the centre of momentum frame of the $p\text{Pb}$ system and so eqn. (2) should be adjusted. For the case where the vector meson is detected at positive rapidities (corresponding to the configurations in the upper row of Fig. 9),

$$W_+^2 = M_V \sqrt{s} e^{+(Y_{\text{lab}} - Y_0)} = W_p^2 \quad \text{and} \quad W_-^2 = M_V \sqrt{s} e^{-(Y_{\text{lab}} - Y_0)} = W_{\text{Pb}}^2, \quad (34)$$

where $Y_0 = 0.465$ is the shift of the nucleon-nucleon centre of mass with respect to the laboratory frame.

Acknowledgements

We thank Petja Paakkinen for providing the numerical values for the EPPS16 gluon modification factor at the scales $\mu^2 = m_c^2$ and $\mu^2 = m_b^2$ used in this work. CAF is supported by the Helsinki Institute of Physics core funding project QCD-THEORY. SPJ is supported by a Royal Society University Research Fellowship (Grant URF/R1/201268). The work of TT is supported by the STFC Consolidated Grant ST/T000988/1. This work is also supported in part by the STFC Grant ST/T001011/1.

Y_{lab}	W_{Pb} (GeV)	f_{Pb}	W_p (GeV)	f_{incoh}	f_{coh}	$f_{\text{incoh}} + f_{\text{coh}}$	$f_{\text{incoh}} + f_{\text{coh}}(R_A = 1)$
-5.125	3570	0.464×10^{-12}	13.31	6.23	0.0	6.23	7.16
-4.875	3150	0.577×10^{-10}	15.08	5.77	0.52×10^{-21}	5.77	6.91
-4.625	2780	0.930×10^{-8}	17.09	6.37	0.22×10^{-10}	6.37	6.66
-4.375	2450	0.725×10^{-6}	19.37	6.83	0.51×10^{-5}	6.83	6.41
-4.125	2160	0.262×10^{-4}	21.95	7.11	0.39×10^{-2}	7.11	6.16
-3.875	1910	0.481×10^{-3}	24.87	7.21	0.15	7.36	6.03
-3.625	1690	0.500×10^{-2}	28.18	7.17	1.2	8.35	6.60
-3.375	1490	0.326×10^{-1}	31.93	7.03	3.9	10.9	8.38
-3.125	1310	0.146	36.18	6.75	7.5	14.2	10.9
-2.875	1160	0.482	41.00	6.29	11	16.8	13.2
-2.625	1020	1.26	46.46	5.64	12	17.8	14.7
-2.375	902	2.71	52.64	4.97	12	17.4	15.5
-2.125	796	5.03	59.65	4.36	12	16.3	15.6
-1.875	703	8.33	67.60	3.81	11	14.9	15.4
-1.625	620	12.6	76.60	3.35	10	13.4	14.8
-1.375	547	17.7	86.80	2.96	9.1	12.1	14.1
-1.125	483	23.5	98.35	2.64	8.2	10.9	13.3
-0.875	426	29.9	111.45	2.36	7.4	9.77	12.4
-0.625	376	36.7	126.29	2.11	6.7	8.79	11.5
-0.375	332	43.8	143.10	1.89	6.0	7.91	10.6
-0.125	293	51.2	162.16	1.69	5.4	7.09	9.74
0.125	258	58.6	183.75	1.51	4.8	6.33	8.83
0.375	228	66.2	208.21	1.33	4.3	5.61	7.94
0.625	201	73.9	235.94	1.17	3.8	4.93	7.06
0.875	178	81.6	267.35	1.02	3.3	4.29	6.21
1.125	157	89.4	302.95	0.88	2.8	3.68	5.37
1.375	138	97.2	343.29	0.74	2.4	3.11	4.58
1.625	122	105	389.00	0.62	1.9	2.57	3.82
1.875	108	113	440.79	0.51	1.6	2.08	3.11
2.125	95.1	121	499.48	0.40	1.2	1.63	2.46
2.375	83.9	128	565.99	0.31	0.93	1.24	1.88
2.625	74.0	136	641.35	0.23	0.67	0.903	1.38
2.875	65.3	144	726.74	0.17	0.46	0.630	0.971
3.125	57.7	152	823.50	0.12	0.30	0.419	0.650
3.375	50.9	160	933.15	0.08	0.19	0.266	0.415
3.625	44.9	167	1057.40	0.05	0.11	0.161	0.253
3.875	39.6	175	1198.19	0.03	0.60×10^{-1}	0.939×10^{-1}	0.149
4.125	35.0	183	1357.73	0.02	0.32×10^{-1}	0.535×10^{-1}	0.852×10^{-1}
4.375	30.9	191	1538.51	0.01	0.16×10^{-1}	0.300×10^{-1}	0.480×10^{-1}
4.625	27.2	199	1743.36	0.01	0.80×10^{-2}	0.165×10^{-1}	0.267×10^{-1}
4.875	24.0	206	1975.48	0.01	0.38×10^{-2}	0.892×10^{-2}	0.145×10^{-1}
5.125	21.2	214	2238.52	0.00	0.18×10^{-2}	0.459×10^{-2}	0.749×10^{-2}

Table 1: The effective photon flux f_{Pb} and $f_{\text{incoh}}, f_{\text{coh}}$ radiated in the case of Υ production at proton-nucleon collision energy $\sqrt{s_{pN}} = 5.02$ TeV by the lead ion and by the proton beam.

Y_{lab}	W_{Pb} (GeV)	f_{Pb}	W_p (GeV)	f_{incoh}	f_{coh}	$f_{\text{incoh}} + f_{\text{coh}}$	$f_{\text{incoh}} + f_{\text{coh}}(R_A = 1)$
-5.125	2040	0.102×10^{-3}	7.62	5.68	0.18×10^{-1}	5.70	4.16
-4.875	1800	0.145×10^{-2}	8.63	5.50	0.29	5.79	4.06
-4.625	1590	0.121×10^{-1}	9.78	5.21	1.3	6.54	4.49
-4.375	1400	0.662×10^{-1}	11.08	4.80	3.1	7.90	5.44
-4.125	1240	0.257	12.56	4.10	4.5	8.63	6.41
-3.875	1090	0.759	14.23	3.31	5.0	8.30	7.03
-3.625	964	1.81	16.12	2.55	4.6	7.17	7.21
-3.375	851	3.63	18.27	1.93	3.9	5.80	7.04
-3.125	751	6.38	20.70	1.46	3.1	4.58	6.65
-2.875	663	10.1	23.46	1.12	2.5	3.58	6.13
-2.625	585	14.7	26.58	0.87	1.9	2.80	5.56
-2.375	516	20.2	30.12	0.69	1.5	2.22	4.98
-2.125	455	26.2	34.13	0.56	1.2	1.78	4.42
-1.875	402	32.8	38.68	0.47	1.0	1.46	3.89
-1.625	355	39.8	43.83	0.39	0.82	1.21	3.40
-1.375	313	47.0	49.66	0.34	0.68	1.02	2.95
-1.125	276	54.4	56.27	0.29	0.57	0.860	2.54
-0.875	244	61.9	63.77	0.25	0.48	0.733	2.18
-0.625	215	69.5	72.26	0.22	0.40	0.626	1.85
-0.375	190	77.2	81.88	0.20	0.34	0.535	1.57
-0.125	168	84.9	92.78	0.17	0.28	0.456	1.32
0.125	148	92.7	105.13	0.15	0.24	0.389	1.11
0.375	130	100	119.13	0.13	0.20	0.330	0.922
0.625	115	108	134.99	0.12	0.16	0.279	0.764
0.875	102	116	152.97	0.10	0.13	0.235	0.630
1.125	89.7	124	173.34	0.09	0.11	0.197	0.517
1.375	79.1	132	196.42	0.08	0.86×10^{-1}	0.164	0.423
1.625	69.8	139	222.57	0.07	0.69×10^{-1}	0.136	0.344
1.875	61.6	147	252.20	0.06	0.54×10^{-1}	0.112	0.279
2.125	54.4	155	285.78	0.05	0.42×10^{-1}	0.918×10^{-1}	0.225
2.375	48.0	163	323.83	0.04	0.33×10^{-1}	0.748×10^{-1}	0.181
2.625	42.4	170	366.95	0.04	0.25×10^{-1}	0.605×10^{-1}	0.145
2.875	37.4	178	415.81	0.03	0.19×10^{-1}	0.486×10^{-1}	0.115
3.125	33.0	186	471.18	0.02	0.14×10^{-1}	0.388×10^{-1}	0.911×10^{-1}
3.375	29.1	194	533.91	0.02	0.11×10^{-1}	0.307×10^{-1}	0.717×10^{-1}
3.625	25.7	202	605.00	0.02	0.78×10^{-2}	0.242×10^{-1}	0.562×10^{-1}
3.875	22.7	209	685.56	0.01	0.56×10^{-2}	0.190×10^{-1}	0.437×10^{-1}
4.125	20.0	217	776.84	0.01	0.40×10^{-2}	0.148×10^{-1}	0.339×10^{-1}
4.375	17.7	225	880.27	0.01	0.29×10^{-2}	0.114×10^{-1}	0.262×10^{-1}
4.625	15.6	233	997.48	0.01	0.20×10^{-2}	0.884×10^{-2}	0.202×10^{-1}
4.875	13.8	240	1130.29	0.01	0.14×10^{-2}	0.673×10^{-2}	0.154×10^{-1}
5.125	12.1	248	1280.79	0.00	0.96×10^{-3}	0.505×10^{-2}	0.116×10^{-1}

Table 2: The effective photon flux f_{Pb} and $f_{\text{incoh}}, f_{\text{coh}}$ radiated in the case of J/ψ production at proton-nucleon collision energy $\sqrt{s_{pN}} = 5.02$ TeV by the lead ion and by the proton beam.

Y_{lab}	W_{Pb} (GeV)	f_{Pb}	W_p (GeV)	f_{incoh}	f_{coh}	$f_{\text{incoh}} + f_{\text{coh}}$	$f_{\text{incoh}} + f_{\text{coh}}(R_A = 1)$
-5.125	4550	0.548×10^{-8}	16.97	7.14	0.90×10^{-11}	7.14	7.52
-4.875	4010	0.482×10^{-6}	19.23	7.70	0.35×10^{-5}	7.70	7.27
-4.625	3540	0.190×10^{-4}	21.79	8.07	0.33×10^{-2}	8.07	7.02
-4.375	3130	0.374×10^{-3}	24.69	8.22	0.15	8.37	6.88
-4.125	2760	0.410×10^{-2}	27.98	8.22	1.2	9.47	7.49
-3.875	2430	0.279×10^{-1}	31.70	8.11	4.2	12.3	9.51
-3.625	2150	0.129	35.92	7.85	8.4	16.3	12.4
-3.375	1900	0.437	40.70	7.37	12	19.5	15.2
-3.125	1670	1.16	46.12	6.65	14	20.8	17.2
-2.875	1480	2.54	52.26	5.92	15	20.7	18.3
-2.625	1300	4.78	59.22	5.23	14	19.5	18.7
-2.375	1150	7.99	67.11	4.61	13	18.0	18.5
-2.125	1010	12.2	76.04	4.08	12	16.4	18.0
-1.875	896	17.2	86.17	3.65	11	14.9	17.4
-1.625	790	23.0	97.64	3.28	10	13.6	16.6
-1.375	697	29.3	110.64	2.97	9.4	12.4	15.7
-1.125	615	36.1	125.38	2.69	8.6	11.3	14.8
-0.875	543	43.2	142.07	2.45	7.9	10.3	13.9
-0.625	479	50.5	160.99	2.23	7.2	9.43	12.9
-0.375	423	58.0	182.42	2.03	6.6	8.60	12.0
-0.125	373	65.6	206.71	1.84	6.0	7.82	11.1
0.125	329	73.2	234.23	1.67	5.4	7.07	10.1
0.375	291	80.9	265.42	1.50	4.9	6.37	9.21
0.625	257	88.7	300.76	1.34	4.4	5.69	8.31
0.875	226	96.5	340.81	1.19	3.9	5.04	7.43
1.125	200	104	386.19	1.04	3.4	4.42	6.57
1.375	176	112	437.61	0.91	2.9	3.83	5.73
1.625	156	120	495.87	0.78	2.5	3.27	4.93
1.875	137	128	561.90	0.65	2.1	2.75	4.17
2.125	121	135	636.72	0.54	1.7	2.26	3.45
2.375	107	143	721.49	0.44	1.4	1.81	2.79
2.625	94.4	151	817.56	0.35	1.1	1.41	2.19
2.875	83.3	159	926.42	0.27	0.79	1.06	1.66
3.125	73.5	167	1049.77	0.20	0.57	0.766	1.20
3.375	64.9	174	1189.54	0.14	0.39	0.530	0.837
3.625	57.2	182	1347.93	0.10	0.25	0.348	0.555
3.875	50.5	190	1527.40	0.07	0.15	0.219	0.351
4.125	44.6	198	1730.77	0.04	0.87×10^{-1}	0.132	0.212
4.375	39.3	206	1961.22	0.03	0.48×10^{-1}	0.766×10^{-1}	0.124
4.625	34.7	213	2222.35	0.02	0.25×10^{-1}	0.435×10^{-1}	0.710×10^{-1}
4.875	30.6	221	2518.26	0.01	0.13×10^{-1}	0.244×10^{-1}	0.400×10^{-1}
5.125	27.0	229	2853.56	0.01	0.62×10^{-2}	0.135×10^{-1}	0.222×10^{-1}

Table 3: The effective photon flux f_{Pb} and $f_{\text{incoh}}, f_{\text{coh}}$ radiated in the case of Υ production at proton-nucleon collision energy $\sqrt{s_{pN}} = 8.16$ TeV by the lead ion and by the proton beam.

Y_{lab}	W_{Pb} (GeV)	f_{Pb}	W_p (GeV)	f_{incoh}	f_{coh}	$f_{\text{incoh}} + f_{\text{coh}}$	$f_{\text{incoh}} + f_{\text{coh}}(R_A = 1)$
-5.125	2600	0.102×10^{-1}	9.71	5.80	1.4	7.19	4.94
-4.875	2300	0.577×10^{-1}	11.00	5.37	3.3	8.70	5.99
-4.625	2030	0.230	12.47	4.63	5.0	9.62	7.11
-4.375	1790	0.695	14.13	3.76	5.6	9.36	7.86
-4.125	1580	1.68	16.01	2.91	5.2	8.15	8.11
-3.875	1390	3.43	18.14	2.21	4.4	6.64	7.97
-3.625	1230	6.10	20.55	1.68	3.6	5.27	7.56
-3.375	1080	9.73	23.29	1.30	2.8	4.13	7.01
-3.125	957	14.3	26.39	1.01	2.2	3.25	6.39
-2.875	845	19.7	29.90	0.80	1.8	2.57	5.76
-2.625	746	25.7	33.89	0.66	1.4	2.09	5.14
-2.375	658	32.2	38.40	0.55	1.2	1.72	4.55
-2.125	581	39.2	43.51	0.46	0.97	1.43	4.00
-1.875	512	46.4	49.30	0.40	0.81	1.21	3.49
-1.625	452	53.7	55.87	0.34	0.68	1.03	3.03
-1.375	399	61.3	63.31	0.30	0.58	0.880	2.62
-1.125	352	68.9	71.74	0.27	0.49	0.758	2.25
-0.875	311	76.6	81.29	0.24	0.42	0.653	1.92
-0.625	274	84.3	92.11	0.21	0.35	0.562	1.63
-0.375	242	92.0	104.37	0.19	0.30	0.484	1.38
-0.125	214	99.8	118.27	0.17	0.25	0.415	1.16
0.125	188	108	134.02	0.15	0.21	0.356	0.974
0.375	166	115	151.86	0.13	0.17	0.303	0.814
0.625	147	123	172.08	0.12	0.14	0.258	0.678
0.875	130	131	195.00	0.10	0.12	0.218	0.564
1.125	114	139	220.96	0.09	0.95×10^{-1}	0.184	0.467
1.375	101	146	250.38	0.08	0.77×10^{-1}	0.155	0.387
1.625	89.0	154	283.72	0.07	0.62×10^{-1}	0.130	0.319
1.875	78.6	162	321.50	0.06	0.49×10^{-1}	0.109	0.263
2.125	69.3	170	364.30	0.05	0.39×10^{-1}	0.904×10^{-1}	0.217
2.375	61.2	178	412.81	0.04	0.31×10^{-1}	0.750×10^{-1}	0.178
2.625	54.0	185	467.77	0.04	0.24×10^{-1}	0.619×10^{-1}	0.145
2.875	47.7	193	530.06	0.03	0.19×10^{-1}	0.508×10^{-1}	0.119
3.125	42.1	201	600.63	0.03	0.14×10^{-1}	0.416×10^{-1}	0.963×10^{-1}
3.375	37.1	209	680.61	0.02	0.11×10^{-1}	0.338×10^{-1}	0.778×10^{-1}
3.625	32.8	216	771.23	0.02	0.83×10^{-2}	0.273×10^{-1}	0.627×10^{-1}
3.875	28.9	224	873.92	0.02	0.62×10^{-2}	0.219×10^{-1}	0.501×10^{-1}
4.125	25.5	232	990.28	0.01	0.46×10^{-2}	0.174×10^{-1}	0.398×10^{-1}
4.375	22.5	240	1122.13	0.01	0.33×10^{-2}	0.138×10^{-1}	0.315×10^{-1}
4.625	19.9	248	1271.54	0.01	0.24×10^{-2}	0.108×10^{-1}	0.248×10^{-1}
4.875	17.5	255	1440.85	0.01	0.17×10^{-2}	0.852×10^{-2}	0.195×10^{-1}
5.125	15.5	263	1632.69	0.01	0.12×10^{-2}	0.663×10^{-2}	0.152×10^{-1}

Table 4: The effective photon flux f_{Pb} and $f_{\text{incoh}}, f_{\text{coh}}$ radiated in the case of J/ψ production at proton-nucleon collision energy $\sqrt{s_{pN}} = 8.16$ TeV by the lead ion and by the proton beam.

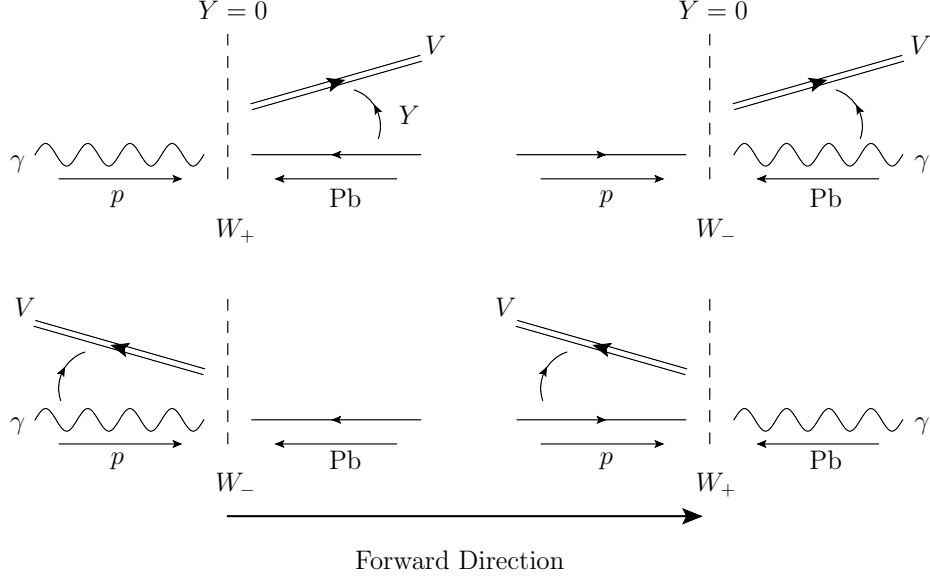


Figure 9: The four kinematic configurations for exclusive heavy vector meson, V , ultraperipheral production in $p\text{Pb}$ collisions at a given rapidity Y occurring via a photoproduction subprocess at two energies, W_+ and W_- . The incoming photon is a Weizsäcker-Williams photon that has been emitted from a proton (lead nucleus) and interacts with an incoming lead nucleus (proton). The vector meson can travel in the direction of the photon (W_+), or against the direction of the photon (W_-).

References

- [1] D. Yu. Ivanov, A. Schafer, L. Szymanowski, and G. Krasnikov. Exclusive photoproduction of a heavy vector meson in QCD. *Eur. Phys. J. C*, **34**(3):297–316, 2004. [Erratum: *Eur. Phys. J. C*, **75**:75, 2015].
- [2] S. P. Jones, A. D. Martin, M. G. Ryskin, and T. Teubner. The exclusive J/ψ process at the LHC tamed to probe the low x gluon. *Eur. Phys. J. C*, **76**(11):633, 2016.
- [3] E. Iancu, K. Itakura, and S. Munier. Saturation and BFKL dynamics in the HERA data at small x . *Phys. Lett. B*, 590:199–208, 2004.
- [4] H. Kowalski, L. Motyka, and G. Watt. Exclusive diffractive processes at HERA within the dipole picture. *Phys. Rev. D*, 74:074016, 2006.
- [5] S. P. Jones, A. D. Martin, M. G. Ryskin, and T. Teubner. Exclusive J/ψ production at the LHC in the k_T factorization approach. *J. Phys. G*, **44**(3):03LT01, 2017.
- [6] V. Guzey and M. Zhalov. Rapidity and momentum transfer distributions of coherent J/ψ photoproduction in ultraperipheral $p\text{Pb}$ collisions at the LHC. *JHEP*, **02**:046, 2014.

- [7] A. G. Shuvaev, K. J. Golec-Biernat, A. D. Martin, and M. G. Ryskin. Off diagonal distributions fixed by diagonal partons at small x and ξ . *Phys. Rev. D*, **60**:014015, 1999.
- [8] A. Shuvaev. Solution of the off forward leading logarithmic evolution equation based on the Gegenbauer moments inversion. *Phys. Rev. D*, **60**:116005, 1999.
- [9] S. Bailey, T. Cridge, L. A. Harland-Lang, A. D. Martin, and R. S. Thorne. Parton distributions from LHC, HERA, Tevatron and fixed target data: MSHT20 PDFs. *Eur. Phys. J. C*, **81**(4):341, 2021.
- [10] C. A. Flett, S. P. Jones, A. D. Martin, M. G. Ryskin, and T. Teubner. How to include exclusive J/ψ production data in global PDF analyses. *Phys. Rev. D*, **101**(9):094011, 2020.
- [11] Roel Aaij et al. Updated measurements of exclusive J/ψ and $\psi(2S)$ production cross-sections in pp collisions at $\sqrt{s} = 7$ TeV. *J. Phys. G*, **41**:055002, 2014.
- [12] Roel Aaij et al. Central exclusive production of J/ψ and $\psi(2S)$ mesons in pp collisions at $\sqrt{s} = 13$ TeV. *JHEP*, **10**:167, 2018.
- [13] C. A. Flett, S. P. Jones, A. D. Martin, M. G. Ryskin, and T. Teubner. Predictions of exclusive Υ photoproduction at the LHC and future colliders. *Phys. Rev. D*, **105**(3):034008, 2022.
- [14] V. M. Budnev, I. F. Ginzburg, G. V. Meledin, and V. G. Serbo. The Two photon particle production mechanism. Physical problems. Applications. Equivalent photon approximation. *Phys. Rept.*, **15**:181–281, 1975.
- [15] V. A. Khoze, A. D. Martin, and M. G. Ryskin. Multiple interactions and rapidity gap survival. *J. Phys. G*, **45**(5):053002, 2018.
- [16] L. A. Harland-Lang, V. A. Khoze, A. D. Martin, and M. G. Ryskin. Searching for the Odderon in Ultraperipheral Proton–Ion Collisions at the LHC. *Phys. Rev. D*, **99**(3):034011, 2019.
- [17] L. A. Harland-Lang, V. A. Khoze, and M. G. Ryskin. Exclusive LHC physics with heavy ions: SuperChic 3. *Eur. Phys. J. C*, **79**(1):39, 2019.
- [18] M. Vidovic, M. Greiner, C. Best, and G. Soff. Impact parameter dependence of the electromagnetic particle production in ultrarelativistic heavy ion collisions. *Phys. Rev. C*, **47**:2308–2319, 1993.
- [19] J. J. Sakurai. Theory of strong interactions. *Annals Phys.*, **11**:1–48, 1960.
- [20] T. H. Bauer, R. D. Spital, D. R. Yennie, and F. M. Pipkin. The Hadronic Properties of the Photon in High-Energy Interactions. *Rev. Mod. Phys.*, **50**:261, 1978. [Erratum: *Rev. Mod. Phys.*, **51**:407, 1979].

- [21] V. A. Khoze, A. D. Martin, and M. G. Ryskin. Exclusive vector meson production in heavy ion collisions. *J. Phys. G*, **46**(8):085002, 2019.
- [22] B. Z. Kopeliovich, L. I. Lapidus, and A. B. Zamolodchikov. Dynamics of Color in Hadron Diffraction on Nuclei. *JETP Lett.*, **33**:595–597, 1981.
- [23] G. Bertsch, S. J. Brodsky, A. S. Goldhaber, and J. F. Gunion. Diffractive Excitation in QCD. *Phys. Rev. Lett.*, **47**:297, 1981.
- [24] B. Alessandro et al. J/ψ and ψ' production and their normal nuclear absorption in proton-nucleus collisions at 400 GeV. *Eur. Phys. J. C*, **48**:329, 2006.
- [25] V. S. Fadin and L. N. Lipatov. BFKL pomeron in the next-to-leading approximation. *Phys. Lett. B*, **429**:127–134, 1998.
- [26] M. Ciafaloni and G. Camici. Energy scale(s) and next-to-leading BFKL equation. *Phys. Lett. B*, **430**:349–354, 1998.
- [27] G. P. Salam. A Resummation of large subleading corrections at small x . *JHEP*, **07**:019, 1998.
- [28] M. Ciafaloni and D. Colferai. The BFKL equation at next-to-leading level and beyond. *Phys. Lett. B*, **452**:372–378, 1999.
- [29] G. Antchev et al. Measurement of elastic pp scattering at $\sqrt{s} = 8$ TeV in the Coulomb–nuclear interference region: determination of the ρ -parameter and the total cross-section. *Eur. Phys. J. C*, **76**(12):661, 2016.
- [30] H. Stenzel. Measurement of the total cross section at 8 TeV and the inelastic cross section at 13 TeV at the LHC with the ATLAS detector. *AIP Conf. Proc.*, **1819**(1):040005, 2017.
- [31] K. J. Eskola, P. Paakkinen, H. Paukkunen, and C. A. Salgado. EPPS16: Nuclear parton distributions with LHC data. *Eur. Phys. J. C*, **77**(3):163, 2017.
- [32] B. B. Abelev et al. Exclusive J/ψ photoproduction off protons in ultra-peripheral $p\text{Pb}$ collisions at $\sqrt{s_{\text{NN}}} = 5.02$ TeV. *Phys. Rev. Lett.*, **113**(23):232504, 2014.
- [33] S. Acharya et al. Energy dependence of exclusive J/ψ photoproduction off protons in ultra-peripheral $p\text{Pb}$ collisions at $\sqrt{s_{\text{NN}}} = 5.02$ TeV. *Eur. Phys. J. C*, **79**(5):402, 2019.
- [34] A. M. Sirunyan et al. Measurement of exclusive Υ photoproduction from protons in $p\text{Pb}$ collisions at $\sqrt{s_{\text{NN}}} = 5.02$ TeV. *Eur. Phys. J. C*, **79**(3):277, 2019.
- [35] C. A. Flett, A. D. Martin, M. G. Ryskin, and T. Teubner. Very low x gluon density determined by LHCb exclusive J/ψ data. *Phys. Rev. D*, **102**:114021, 2020.

- [36] Zi-Qiang Chen and Cong-Feng Qiao. NLO QCD corrections to exclusive electroproduction of quarkonium. *Phys. Lett. B*, **797**:134816, 2019. [Erratum: *Phys. Lett. B*, 135759, 2020].
- [37] C. A. Flett, J. A. Gracey, S. P. Jones, and T. Teubner. Exclusive heavy vector meson electroproduction to NLO in collinear factorisation. *JHEP*, **08**:150, 2021.
- [38] G. T. Bodwin, E. Braaten, and G. P. Lepage. Rigorous QCD analysis of inclusive annihilation and production of heavy quarkonium. *Phys. Rev. D*, **51**:1125–1171, 1995. [Erratum: *Phys. Rev. D*, **55**:5853, 1997].
- [39] S. P. Jones, A. D. Martin, M. G. Ryskin, and T. Teubner. Exclusive J/ψ and Υ photoproduction and the low x gluon. *J. Phys. G*, **43**(3):035002, 2016.
- [40] M. G. Ryskin, R. G. Roberts, A. D. Martin, and E. M. Levin. Diffractive J/ψ photoproduction as a probe of the gluon density. *Z. Phys. C*, **76**:231–239, 1997.
- [41] C. Adloff et al. Diffractive photoproduction of $\psi(2S)$ mesons at HERA. *Phys. Lett. B*, **541**:251–264, 2002.
- [42] V. A. Khoze, A. D. Martin, and M. G. Ryskin. Diffraction at the LHC. *Eur. Phys. J. C*, **73**:2503, 2013.
- [43] D. Dutta, K. Naskar, R. Chudasama, and P. Sarin. Study of Upsilon photoproduction in p Pb collisions at 8.16 TeV with CMS experiment. *DAE Symp. Nucl. Phys.*, **62**:964–965, 2017.
- [44] K. Naskar, D. Dutta, and P. Sarin. Background study of Upsilon photoproduction in p Pb collisions at 8.16 TeV with CMS experiment. *DAE Symp. Nucl. Phys.*, **63**:958–959, 2018.
- [45] R. D. Woods and D. S. Saxon. Diffuse Surface Optical Model for Nucleon-Nuclei Scattering. *Phys. Rev.*, **95**:577–578, 1954.
- [46] C. M. Tarbert et al. Neutron skin of ^{208}Pb from Coherent Pion Photoproduction. *Phys. Rev. Lett.*, **112**(24):242502, 2014.
- [47] A. B. Jones and B. A. Brown. Two-parameter Fermi function fits to experimental charge and point-proton densities for ^{208}Pb . *Phys. Rev. C*, **90**(6):067304, 2014.
- [48] K. J. Eskola, C. A. Flett, V. Guzey, T. Löytäinen, and H. Paukkunen. Exclusive J/ψ photoproduction in ultraperipheral Pb+Pb collisions at the LHC to next-to-leading order perturbative QCD. arXiv:2203.11613.